Contrasting trends in short-lived and long-lived mesoscale eddies in the Southern Ocean since the 1990s

F. Shi[1], Y. Luo[2], R. Wu[1], Q. Yang[1], R. Chen[2], C. Wang[1], Y. Lin[1] and D. Chen[1]

[1]School of Atmospheric Sciences, Sun Yat-sen University, and Southern Marine Science and Engineering Guangdong Laboratory (Zhuhai), 519082 Zhuhai, China.

[2] Frontier Science Center for Deep Ocean Multispheres and Earth System (FDOMES), Physical Oceanography Laboratory, and College of Oceanic and Atmospheric Sciences, Ocean University of China, 266100, Qingdao, China.

Corresponding author: Renhao Wu (wurenhao@mail.sysu.edu.cn)

Key Points:

- Long-lived eddies dominate the increasing intensity trend of eddies in the Southern Ocean.
- The amplitude trends of the long-lived and short-lived eddies show nonuniform patterns.
- The increased baroclinic instabilities of mean flows are responsible for the amplitude increase of the long-lived eddies.

Abstract

Mesoscale eddies play an important role in both momentum and heat balances in the Southern Ocean. Previous studies have documented an increasing intensity of the Southern Ocean eddy field during recent decades; however, it is still unclear whether the mesoscale eddies with different lifetimes have different temporal variations. Using satellite altimeter observations from 1993 to 2020, we find that the increasing trend in the intensity of eddies is dominated by long-lived eddies (with lifetimes ≥ 90 days), whose amplitude has increased at a rate of ~2.8% per decade; the increase is concentrated downstream of topography. In contrast, short-lived eddies (with lifetimes < 90 days) do not appear to have a significant trend in their amplitudes since the early 1990s. An energy conversion analysis indicates that the increased baroclinic instabilities of the mean flows associated with topography are responsible for the amplitude increase of the long-lived eddies.

Plain Language Summary

The Southern Ocean is saturated with energetic eddies, which play a central role in modulating the ocean circulation and transporting heat, carbon, and nutrients. Much attention has been paid to the observed increasing trend in the eddy kinetic energy field in recent years; however, trends in the intensity of eddies with different lifetimes have been overlooked. Herein, the mesoscale eddies in the Southern Ocean are separated into two groups, with those with lifetimes shorter than 90 days being defined as short-lived eddies and those with lifetimes longer than 90 days being defined as long-lived eddies. Results show that the increasing intensity trend is dominated by the long-lived eddies. In contrast, the short-lived eddies do not appear to have a significant amplitude trend since the early 1990s. An energy conversion analysis indicates that the increased baroclinic instabilities of the mean flows are responsible for the amplitude increase of the long-lived eddies. This study suggests that eddies with long lifetimes are more sensitive to warming in the Southern Ocean with the accompanying westerly wind strengthening, highlighting the need for better understanding the changes in eddies on separate scales instead of considering them together.

1 Introduction

The Southern Ocean (SO) is a key component of the global climate system that has experienced pronounced subsurface warming alongside westerly wind strengthening in recent decades (Böning et al., 2008; Waugh et al., 2013; Shi et al., 2021). There, mesoscale eddies regulate the Antarctic circumpolar circulation (ACC) and meridional heat exchange, which further influence the transport of heat, carbon, and nutrients (Screen et al., 2009; Chelton et al., 2011; Keppler & Landschützer, 2019; Friedrichs et al., 2022; Morrison et al., 2022). Primarily due to anthropogenic ocean warming and secondarily owing to wind stress strengthening, the ACC has been observed and modeled to undergo robust zonal acceleration (Shi et al., 2020, 2021). The response of the ACC and the upper cell of the circumpolar meridional overturning circulation (MOC) to changes in wind stress were previously explained by two hypotheses: "eddy saturation" and "eddy compensation" (Straub, 1993; Hallberg & Gnanadesikan, 2001; Hallberg & Gnanadesikan, 2006; Hogg et al., 2008; Hogg, 2010; Viebahn & Eden, 2010).

Due to the dynamic importance of mesoscale eddies, much attention has been paid to changes in the eddy kinetic energy (EKE) in the SO since the advent of satellite altimetry (Fu et al., 2010). For example, a robust increase in the EKE field has been observed since 1993, with larger trends in the Pacific and Indian sectors (Meredith & Hogg, 2006; Hogg et al., 2015; Menna et al., 2020). Following Hogg et al. (2015), Martínez-Moreno et al. (2019, 2022) decomposed the eddy field into mesoscale eddies and residual components and demonstrated that the increasing trend of EKE is mainly impacted by mesoscale eddies. Moreover, the EKE field shows a more significant increase of 2-5% per decade in the eddy-rich regions. In comparison, Zhang et al. (2021) pointed out that EKE increases significantly only downstream of the Campbell Plateau rather than in other regions along the ACC. The causes for the long-term changes in the EKE are thought to be due to a strengthening of the wind stress with delays of 1–4 years (Hogg et al., 2015; Menna et al., 2020). Besides external wind-forced changes in the EKE, high-resolution modeling has suggested that the eddy field also exhibited a chaotic internal nature, which may mask wind-driven changes (Meredith, 2016; Patara et al., 2016; Hogg et al., 2022). Another important feature is the spatial pattern of the EKE field, which is collocated with major topography and is primarily determined by the instability of the mean flow (Graham et al., 2012; Barthel et al., 2017; Chapman, 2017; Youngs et al., 2017; Cai et al., 2022). Model experiments showed that the EKE depends on the shape and height of the topography as well as

on the baroclinicity of the jet, but it is not very sensitive to increased wind stress (Barthel et al., 2017; Cai et al., 2022). The nonlinear evolution of the instability leads to an inverse cascade of energy and likely determines the eddy properties (Pedlosky, 1987; Venaille et al., 2011; Scott & Wang, 2005); however, the long-term changes in barotropic and baroclinic instabilities and their connections with eddy variations in the SO remain unexplored.

Previous studies have mainly focused on the EKE field, which includes features like waves, meanders, and eddies of multiple scales; however, it is still unclear whether the mesoscale eddies with different lifetimes temporally differ in their variations. This study investigates how mesoscale eddies with different lifetimes respond to the SO changes and the possible physical processes responsible for those changes. To answer these questions, we explore the long-term trends in mesoscale eddies identified and tracked from satellite altimeter records from 1993 to 2020; we find that the increasing intensity trends are dominated by eddies with longer lifetimes, with the short-lived eddies only contributing slight changes. The mechanism behind this is illustrated by the increasing trends in energy conversion due to baroclinic instability. The remainder of this paper is organized as follows: Section 2 introduces the data and methods, the results are described in Section 3, and the discussion and conclusions are outlined in Section 4.

2 Data and Methods

2.1 Satellite altimeter and sea surface temperature products

The daily surface height (SSH) and derived surface geostrophic speeds have a horizontal resolution of $1/4°$ from 1993 to 2020. Mesoscale eddies with coherent structures are identified and tracked based on the SSH after removing the large-scale variability, and eddy trajectory atlas products (META3.2 DT) are developed (Mason et al., 2014; Pegliasco et al., 2022). In the atlas, the eddy amplitude ($Eddy_{amp}$) is defined as the magnitude of the difference between the extremum of SSH within the eddy and the SSH around the eddy edge, which exhibits a linear relationship with the surface geostrophic speed; the eddy length scale is equal to the diameter of an eddy that has the area of the coherent structure, $L_e = 2\sqrt{area/\pi}$. Details on the eddy characteristics are described in Peliasco et al. (2022).

Mesoscale eddies with lifetimes shorter than 10 days are not considered herein since the resolvable temporal scale of the product is around 10 days (Pujol et al., 2016; Chen & Han, 2019). To reduce noise in the data, eddies with amplitudes smaller than 2 cm are also discarded. The present work divides the eddies into two groups based on their lifetimes. One group consists of short-lived eddies with lifetimes shorter than 90 days but longer than 10 days; The other group consists of long-lived eddies with lifetimes equal to or longer than 90 days. The median lifetime of eddies is around three months, among which the short-lived and long-lived eddies account for 52% and 45% of the totals, respectively (Table S1). Our review of the results indicates that the conclusions of this analysis are not very sensitive to how the short- and long-lived eddies are partitioned (Fig. 1, S2 and S3).

The National Oceanic and Atmospheric Administration (NOAA) Daily Optimum Interpolation Sea Surface Temperature (OISST) incorporates observations from different platforms into a regular global grid (Huang et al., 2021). The OISST v2.1 product has a horizontal resolution of $1/4°$ and is available from September 1981 to the present. We analyze the period of overlap with the eddy trajectory atlas from January 1993 to December 2020.

2.2 Energy conversion

Energy equations provide a quantitative description of the energy exchange between eddies and the mean flow (Cronin & Watts, 1996; Eden & Böning, 2002; Kang & Curchitser, 2015). Through instability processes, eddies can extract energy from the mean flow, where a barotropic conversion process (BT) occurs from the mean kinetic energy (MKE) to the EKE, and a baroclinic conversion process (BC) occurs from the mean potential energy (MPE) to the eddy potential energy (EPE). Due to the lack of long-term salinity observations, following Cronin & Watts (1996), the SST variability is used to represent the approximate density variability in the surface layer, using $\rho = \rho_0(1 - \varphi T)$. The temperature trend at the surface shows a pattern similar to those in the upper SO (Fig. S1), which suggests that the SST is roughly representative of the long-term changes in the upper ocean temperatures. Thus, we calculate the BT and BC in the surface layer as follows:

$$BT = -\rho_0 \left[\overline{u'^2} \frac{\partial \overline{u}}{\partial x} + \overline{v'^2} \frac{\partial \overline{v}}{\partial y} + \overline{u'v'} \left(\frac{\partial \overline{v}}{\partial x} + \frac{\partial \overline{u}}{\partial y} \right) \right], \quad (1)$$

and

$$BC = -\frac{g^2}{\overline{N^2}\rho_0}\left(\overline{u'\rho'}\frac{\partial\overline{\rho}}{\partial x} + \overline{v'\rho'}\frac{\partial\overline{\rho}}{\partial y}\right) = -\frac{\rho_0\alpha g}{\frac{\partial\overline{T}}{\partial z}}\left(\overline{u'T'}\frac{\partial\overline{T}}{\partial x} + \overline{v'T'}\frac{\partial\overline{T}}{\partial y}\right), \quad (2)$$

where $\overline{u}, \overline{v}, \overline{\rho},$ and $\overline{T}$ are the time-mean zonal and meridional velocity, seawater density, and temperature from 1993–2020, respectively; u', v', ρ', and T' are the time-varying zonal and meridional velocity, seawater density, and temperature, respectively. In the equations, g, ρ_0, φ, and N^2 are an acceleration of gravity, a constant density of 1025 kgm^{-3}, thermal expansion, and the buoyancy frequency, respectively. The mesoscale eddies emerge from the barotropic instability of strongly horizontal velocity shear or are generated by baroclinic instability from the collapsing of horizontal density gradients. The BT and BC are direct sources of eddy growth, with positive values indicating eddy formation.

3 Results

3.1 Changes in eddies with different lifetimes

Here, we begin to explore changes in the amplitude ($Eddy_{amp}$) and number ($Eddy_{num}$) of the eddies with different lifetimes over the region between 45°S and 65°S, which roughly covers the ACC path and its surroundings (Figs. 1 and S2). Figure 1a shows that all eddies have increased amplitudes since the early 1990s, with the increase being much more significant for the eddies with lifetimes longer than 90 days. The amplitude increase of the long-lived eddies has reached a rate of 0.26 ± 0.06 cm or $2.8\% \pm 0.6\%$ per decade (Fig. 1c), which is consistent with trends in the EKE (Hogg et al., 2015; Martínez-Moreno et al., 2021), while the amplitude of the short-lived eddies does not appear to have had a significant change during the past a few decades (Fig. 1c). In addition, the variability of the eddies with lifetimes longer than 10 days is collocated with that of the long-lived eddies (Fig. 1c), indicating that the long-lived eddies are largely responsible for the changes and variations in the eddy amplitude in the SO. There is also an increasing trend in the number of eddies that is dominated by the long-lived eddies (Figs. 1b and 1d). These may be a consequence of more long-lived eddies being formed or small eddies merging into larger ones through eddy–eddy interaction (the transfer of energy from small to large scales) (Groom, 2015).

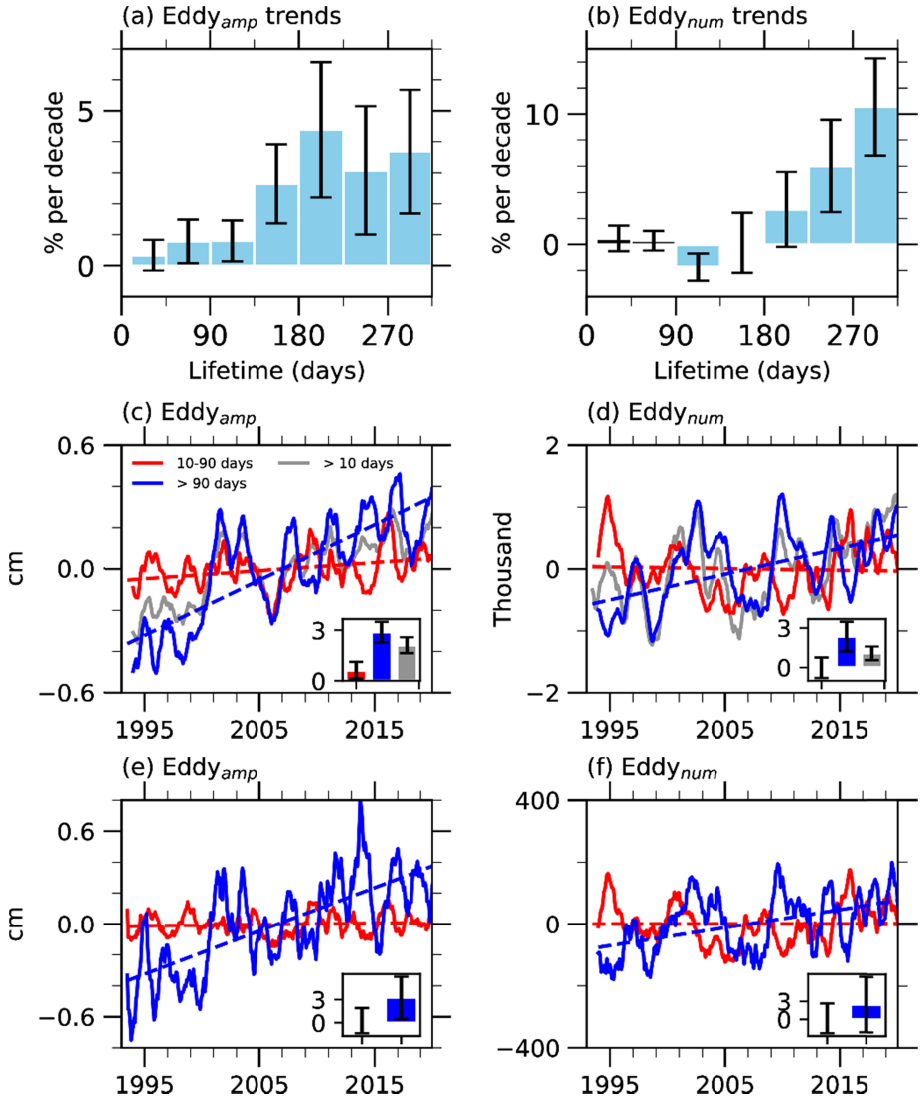

Figure 1. Trends in the (a) amplitude ($Eddy_{amp}$) and (b) number ($Eddy_{num}$) of eddies with different lifetimes in 45-day bins. The error bars denote the standard deviations of the annual mean values. Time series of the (c) $Eddy_{amp}$ and (d) $Eddy_{num}$ anomalies of the short-lived eddies (with lifetimes between 10 and 90 days), long-lived eddies (lifetimes ≥ 90 days), and all eddies (lifetimes > 10 days) in the SO (45°S–65°S). Time series of (e) $Eddy_{amp}$ and (f) $Eddy_{num}$ anomalies of short-lived and long-lived eddies during their growing period (the first 15% of their lifetimes). In (c)–(f), the solid curves are 12-month moving averages, and dashed lines are trends above the 95% confidence level; the insets in the lower right of each panel show the corresponding trends in units of percent per decade.

171 Following Samelson et al. (2014) and Pegliasco et al. (2015), the evolution of a mesoscale
172 eddy is divided into three stages, with 0–15% of its lifetime as the growing phase, 15–85% as the
173 mature phase, and 85–100% as the decaying phase. Because the development of eddies is
174 sourced from the energy of the mean flow, the changes in the amplitude and number of eddies
175 are further explored during their growing phase (Figs. 1e and 1f). The long-lived eddies in the
176 growing phase strengthened at a rate of 0.26 ± 0.2 cm or $3.2\% \pm 2.7\%$ per decade, while the
177 short-lived eddies show small changes in their amplitudes (Fig. 1e). The number of long-lived
178 eddies in the growing phase has increased slightly with a large standard error and is barely
179 significant at the 95% confidence level (Fig. 1f); by comparison, the number of short-lived
180 eddies does not appear to exhibit a significant change. This analysis reveals that much larger
181 increases in the amplitude of the long-lived eddies than in the short-lived eddies may be induced
182 by more energy extraction in the growing period.

183 3.2 Spatial features of the trends

184 The spatial distribution of eddies suggests that eddy generation in the SO is not uniform but
185 is centralized around five hotspots. Considering Figs. 2a–c, the five hot spots of eddies are all
186 located downstream of major topographic features along the ACC, which is consistent with the
187 findings of previous studies (e.g., Zajaczkovski, 2017). While the five hotspots of the long-lived
188 eddies are collocated with those of the short-lived eddies, the long-lived eddies are distributed
189 more widely due to their ability to propagate farther away (Figs. 2b and 2c). Figures 2d and 2e
190 show that the trends in the amplitudes of the eddies are highly heterogeneous along the ACC,
191 with larger trends concentrated in the eddy-rich area downstream of the topography. The
192 increasing trend in the amplitude of the eddies is dominated by the long-lived eddies, whose
193 amplitude has increased at a rate of up to 0.3 cm per decade. In contrast, the short-lived eddies
194 appear to have a much weaker increasing trend in their amplitudes. These spatial variations may
195 reflect the impacts of local wind stress or interactions between the ACC and local topography
196 (Thompson & Garabato, 2014; Hogg et al., 2015; Rintoul, 2018).

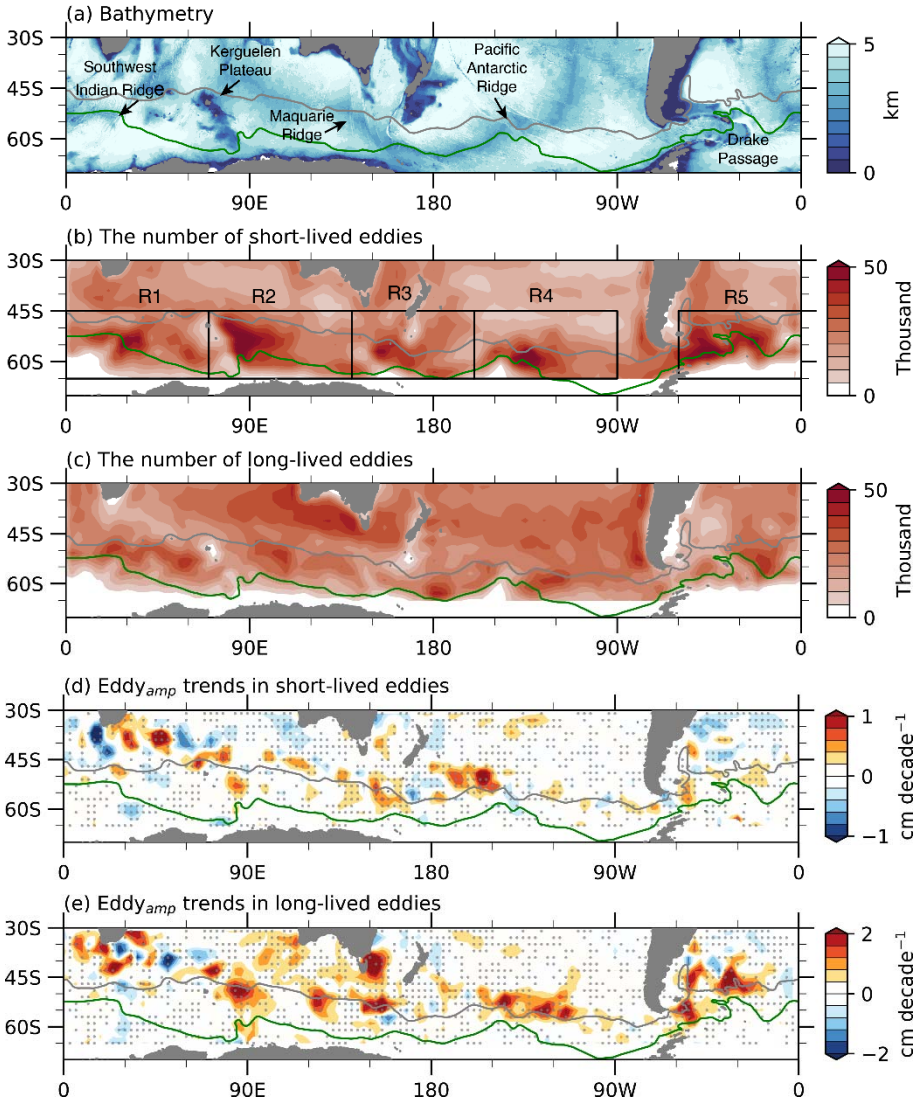

197

198 **Figure 2.** (a) The bathymetry, the number of (b) short-lived and (c) long-lived eddies, and the
199 amplitude trend of (d) short-lived and (e) long-lived eddies in 6° × 4° bins. The gray stippling
200 indicates that the trends are statistically significant at the 95% confidence level. The curves
201 indicate the Subantarctic Front (gray contour) and Southern ACC Front (green contour),
202 respectively (Orsi et al., 1995). The five eddy-rich regions (R1: $0-70°$E, R2: $70-140°$E, R3:
203 $140-200°$E, R4: $200-270°$E, and R5: $300-360°$E) are defined from west to east
204 meridionally between 45°S and 65°S to cover the main ACC path. The five major topographic
205 features are the Southwest Indian Ridge (SWIR), Kerguelen Plateau (KP), Maquarie Ridge
206 (MR), Pacific Antarctic Ridge (PAR), and Drake Passage (DP).

207

208 To further explore changes in the amplitudes of short-lived and long-lived eddies in the
209 eddy-rich regions (Figure S4), we divide the main ACC path into five subregions, each roughly
210 covering one hotspot of eddies (Figure 2b). The amplitudes of long-lived eddies have increased
211 significantly above the 95% confidence level in the R2 − R5, with the largest trends in the R2 at
212 a rate of ~0.3 cm or 3.5% per decade, while the amplitude of long-lived eddies appears to
213 slightly decrease in the R1 at a rate of $0.9\% \pm 0.6\%$ per decade. In contrast, the amplitudes of
214 short-lived eddies show no robust trends in the R1, R2, R3, and R5, barely significantly above
215 the 95% confidence level, but they show a weak increasing trend in the R4 at a rate of
216 ~0.1 cm or 1.7% per decade. The contrasting trends in the eddy amplitudes in the five hotspots
217 are consistent with the changes in the EKE field (Martínez-Moreno et al., 2021, 2022), indicating
218 the importance of local dynamics, such as local wind stresses and interactions between the mean
219 flow and local topography (Rintoul, 2018).

220 3.3 Mechanism for the trends in the eddy amplitudes

221 The above analysis finds that the mesoscale eddies have increasing amplitude trends in the
222 SO, with the trend being more significant for the long-lived eddies in several hotspots along the
223 ACC (Fig. 2e). Around the five eddy-rich regions along the ACC jet, there appears to be positive
224 mean energy conversion from the MKE to the EKE (BT) due to barotropic instabilities of the
225 mean flow (Fig. S5), which is consistent with the distribution of the energetic eddy field. The BT
226 is small near the Southwest Indian Ridge (SWIR) but large near the Kerguelen Plateau (KP),
227 Maquarie Ridge (MR), Pacific Antarctic Ridge (PAR), and Drake Passage (DP), with the
228 maximum reaching $\sim 1 - 5 \times 10^{-4}\, Wm^{-2}$. The energy conversion from the MPE to the EPE
229 (BC) due to baroclinic instabilities is also centralized around the eddy-rich regions, and its value
230 is much larger than that of the BT, reaching $\sim 5 - 10 \times 10^{-4}\, Wm^{-2}$, which indicates more
231 energy is being released from the baroclinic instabilities. Moreover, the locations of the elevated
232 eddy energy and the BC coincide with the bottom topography but not with those of strengthened
233 winds, which implies the primary role of topography in shaping eddy activity patterns along the
234 ACC (e.g., Graham et al., 2012; Thompson & Sallée, 2012; Barthel et al., 2017; Cai et al., 2022).
235

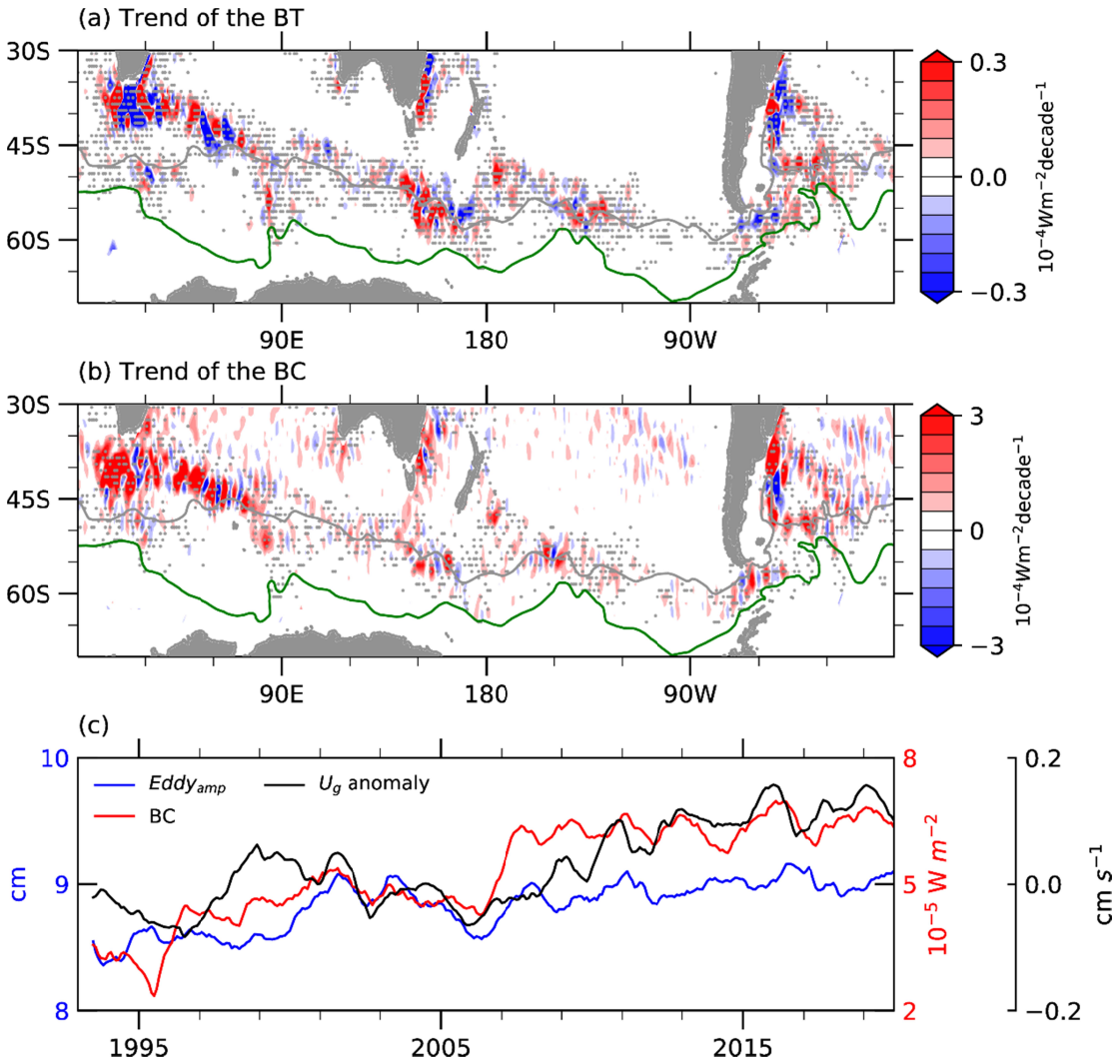

Figure 3. Trends in the (a) barotropic and (b) baroclinic energy conversion in the surface layer. The gray stippling indicates that the trends are statistically significant at the 95% confidence level. (c) Time series of the amplitude of the long-lived eddies (blue curve), the BC in the surface layer (red curve), and the surface zonal geostrophic velocity U_g anomaly (black curve) averaged between 45°N and 65°N.

Both the BT and BC have increased significantly around the five eddy-rich regions since the early 1990s, with the trend for the latter being much larger than that for the former (Figs. 3a and 3b). The pattern of the BC trend agrees well with the topography, with a maximum of $\sim 3 \times 10^{-4}\, Wm^{-2}$ per decade (Fig. 3b). The long-term change in the BC is correlated well with a surface-accelerated zonal geostrophic velocity with a correlation coefficient of 0.64 (Fig. 3c). The close link of the BC to the topography indicates that the BC is sourced from interactions

between the accelerated mean flow and topography. Meanwhile, the amplitude change of the long-lived eddies is highly significantly correlated with the change in the BC, with a correlation coefficient of 0.79 and a lag of three months, suggesting that baroclinic instability is the main process providing the energy for increasing the intensity of the eddies. But why these long-lived eddies? According to Scott & Wang (2005) and Tulloch et al. (2011), the most unstable scale of instabilities has a wavelength a few times larger than the deformation radius, which is ~100 km along the ACC path, as estimated from linear instability theory, $2\pi L_d$, where L_d is the first Rossby radius of deformation (Fig. S6). In other words, the maximum perturbation energy can be expected at a scale of ~100 km. On the other hand, the mean length scales of long-lived eddies when they are detected for the first time are about $90 - 100$ km, which corresponds well to the most unstable scale, while the length scales of short-lived eddies are much smaller. Therefore, increased baroclinic instabilities support amplitude increases of the long-lived eddies whose scale is near that of the energy source in the SO.

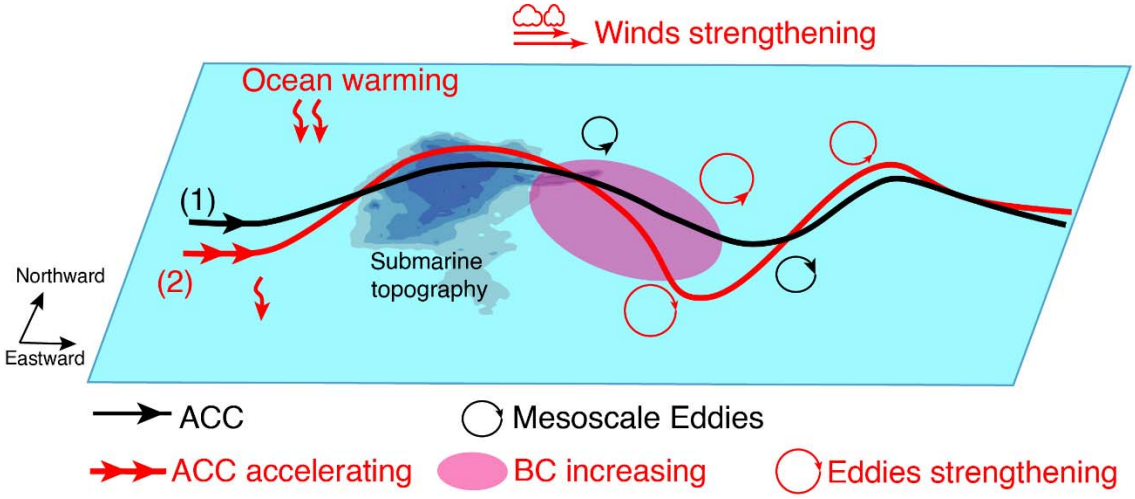

Figure 4. Schematic diagram of possible physical processes underlying the eddy amplitude increase along the ACC path. Red curves and text indicate the changes from a reference state (black curves) in response to the SO warming and an increase in wind stress. (1) The ACC interacts with topography, which shapes the features of the elevated eddy field downstream of the topography. (2) In response to the SO warming and the westerly wind strengthening, the ACC undergoes zonal acceleration, the meander curvature increases, and meridional density gradients become greater. As a consequence, the BC of the mean flow significantly increases

271 there, driving the amplitude increase of eddies with longer lifetimes whose scales are near the
272 most unstable scale.

273 **4 Discussion and Conclusions**

274 Our findings identified long-lived eddies that have dominated the increasing eddy intensity
275 trend based on satellite altimeter observations from 1993 to 2020 in the SO; the increased
276 baroclinic instabilities responsible for these long-term changes along the ACC path (between
277 45°S and 65°S) were also identified. Moreover, there are substantial longitudinal variations in
278 the eddy amplitude trends, with a larger increase downstream of the major topography. As
279 summarized in the schematic diagram in Fig. 4, the ACC jet is largely zonal upstream of the
280 topography where the eddy energy is relatively low. When the jet encounters the major
281 topography, the water columns are squashed/stretched and move equatorward/poleward, leading
282 to a meander curvature and an unstable flow, which shapes the features of the elevated eddy field
283 downstream of the topography (Barthel et al., 2017; Rintoul, 2018; Cai et al., 2022). Because the
284 SO experienced pronounced warming in recent decades, more (less) warming north (south) of
285 the ACC caused greater isopycnal tilting and robust zonal acceleration (Shi et al., 2021). At the
286 same time, the strengthening westerly winds contributed to isopycnal tilt, while the increased
287 meander curvature adjusted to balance the increased zonal transports (Thompson & Garabato,
288 2014), which resulted in enhanced eddy activities. As a consequence, the BC of the mean flow
289 significantly increased, which is more favorable for releasing available potential energy. These
290 increased instabilities provided favorable conditions for the generation of more energetic eddies
291 with longer lifetimes whose scales are ~90 km.

292 Despite the significant amplitude increases of long-lived eddies, as shown herein, the
293 amplitudes of short-lived eddies have changed little. Given short-lived eddies' lifetimes (defined
294 here as between 10 and 90 days), these results may partly reflect the stochastic, chaotic nature of
295 these eddies (Hogg et al., 2022) and partly represent changes in eddies with relatively long
296 lifetimes. In addition, much of the existing research has indicated that the ocean is saturated with
297 nonlinear eddies that merge, split, and couple with one another (Groom, 2015). We found that
298 the number of long-lived eddies also slightly increased in recent years, but the trend in the
299 number of short-lived eddies was not significant. It seems that more long-lived eddies develop
300 partly from eddy–eddy interaction. Note that we only consider the tracked eddies with lifetimes

larger than 10 days and amplitudes larger than 2 cm. Martínez-Moreno et al. (2019) found a decreasing trend in the number of eddies because they identified transient eddies using different algorithms and a larger area between $30°S - 60°S$.

In summary, the present study indicates that long-lived eddies strengthened at a quicker rate in response to climate change (ocean warming and wind intensification) in the SO, which highlights the need for further understanding the changes in eddies on separate scales instead of considering them together. Due to their ability to propagate farther away, long-lived eddies may play a more important role in transporting heat, carbon, and nutrients in the future (Screen et al., 2009; Chelton et al., 2011; Keppler & Landschützer, 2019).

Acknowledgments

This work was supported by the National Natural Science Foundation of China (No. 42230405, 41976006 and 42006029), the Southern Marine Science and Engineering Guangdong Laboratory (Zhuhai) (Grant SML2021SP302), the Program of Marine Economy Development Special Fund (Six Marine Industries) under Department of Natural Resources of Guangdong Province, (Project No. GDNRC [2022]18).

Open Research

All data used in this study are publicly accessible from these websites: the satellite altimeter products: https://doi.org/10.48670/moi-00148; the eddy trajectory atlas: https://doi.org/10.24400/527896/a01-2022.005.220209; the SST products OISST v.2.1: https://www.ncei.noaa.gov/products/optimum-interpolation-sst. The trend analysis uses xarrayMannKendall (https://doi.org/10.5281/zenodo.4458776).

References

Barthel, A., McC. Hogg, A., Waterman, S., & Keating, S. (2017). Jet-topography interactions affect energy pathways to the deep Southern Ocean. *Journal of Physical Oceanography*, *47*(7). https://doi.org/10.1175/JPO-D-16-0220.1

Böning, C. W., Dispert, A., Visbeck, M., Rintoul, S. R., & Schwarzkopf, F. U. (2008). The response of the antarctic circumpolar current to recent climate change. *Nature Geoscience*. https://doi.org/10.1038/ngeo362

Cai, Y., Chen, D., Mazloff, M. R., Lian, T., & Liu, X. (2022). Topographic Modulation of the Wind Stress Impact on Eddy Activity in the Southern Ocean. *Geophysical Research Letters*, *49*(13), e2022GL097859. https://doi.org/10.1029/2022GL097859

Chapman, C. C. (2017). New perspectives on frontal variability in the Southern Ocean. *Journal of Physical Oceanography*, *47*(5). https://doi.org/10.1175/JPO-D-16-0222.1

Chelton, D. B., Schlax, M. G., & Samelson, R. M. (2011). Global observations of nonlinear mesoscale eddies. *Progress in Oceanography*, *91*(2), 167–216. https://doi.org/10.1016/j.pocean.2011.01.002

Chen, G., & Han, G. (2019). Contrasting Short-Lived With Long-Lived Mesoscale Eddies in the Global Ocean. *Journal of Geophysical Research: Oceans*, *124*(5). https://doi.org/10.1029/2019JC014983

Cronin, M., & Watts, D. R. (1996). Eddy–Mean Flow Interaction in the Gulf Stream at 68°W. Part I: Eddy Energetics. *Journal of Physical Oceanography*, *26*(10), 2107–2131. https://doi.org/10.1175/1520-0485(1996)026<2107:EFIITG>2.0.CO;2

Eden, C., & Böning, C. (2002). Sources of Eddy Kinetic Energy in the Labrador Sea. *Journal of Physical Oceanography*, *32*(12), 3346–3363. https://doi.org/10.1175/1520-0485(2002)032<3346:SOEKEI>2.0.CO;2

Friedrichs, D. M., McInerney, J. B. T., Oldroyd, H. J., Lee, W. S., Yun, S., Yoon, S. T., et al. (2022). Observations of submesoscale eddy-driven heat transport at an ice shelf calving front. *Communications Earth & Environment 2022 3:1*, *3*(1), 1–9. https://doi.org/10.1038/s43247-022-00460-3

Fu, L. L., Chelton, D. B., Le Traon, P. Y., & Morrow, R. (2010). Eddy dynamics from satellite altimetry. *Oceanography*, *23*(4). https://doi.org/10.5670/oceanog.2010.02

Graham, R. M., De Boer, A. M., Heywood, K. J., Chapman, M. R., & Stevens, D. P. (2012). Southern Ocean fronts: Controlled by wind or topography? *Journal of Geophysical Research: Oceans*, *117*(8). https://doi.org/10.1029/2012JC007887

Grooms, I. (2015). A computational study of turbulent kinetic energy transport in barotropic turbulence on the f-plane. *Physics of Fluids*, *27*(10). https://doi.org/10.1063/1.4934623

Hallberg, R., & Gnanadesikan, A. (2001). An exploration of the role of transient eddies in determining the transport of a zonally reentrant current. *Journal of Physical Oceanography*, *31*(11). https://doi.org/10.1175/1520-0485(2001)031<3312:AEOTRO>2.0.CO;2

Hallberg, Robert, & Gnanadesikan, A. (2006). The Role of Eddies in Determining the Structure and Response of the Wind-Driven Southern Hemisphere Overturning: Results from the Modeling Eddies in the Southern Ocean (MESO) Project. *Journal of Physical Oceanography*, *36*(12), 2232–2252. https://doi.org/10.1175/JPO2980.1

Hogg, A. M. C. (2010). An Antarctic Circumpolar Current driven by surface buoyancy forcing. *Geophysical Research Letters*, *37*(23). https://doi.org/10.1029/2010GL044777

Hogg, A. M. C., Meredith, M. P., Blundel, J. R., & Wilson, C. (2008). Eddy heat flux in the Sourthern ocean: Response to variable wind forcing. *Journal of Climate*, *21*(4). https://doi.org/10.1175/2007JCLI1925.1

Hogg, A. M. C., Meredith, M. P., Chambers, D. P., Abrahamsen, E. P., Hughes, C. W., & Morrison, A. K. (2015). Recent trends in the Southern Ocean eddy field. *Journal of Geophysical Research: Oceans*, *120*(1). https://doi.org/10.1002/2014JC010470

Hogg, A. M. C., Penduff, T., Close, S. E., Dewar, W. K., Constantinou, N. C., & Martínez-Moreno, J. (2022). Circumpolar Variations in the Chaotic Nature of Southern Ocean Eddy Dynamics. *Journal of Geophysical Research: Oceans*, *127*(5), e2022JC018440. https://doi.org/10.1029/2022JC018440

Huang, B., Liu, C., Banzon, V., Freeman, E., Graham, G., Hankins, B., et al. (2021). Improvements of the Daily Optimum Interpolation Sea Surface Temperature (DOISST) Version 2.1. *Journal of Climate*, *34*(8). https://doi.org/10.1175/JCLI-D-20-0166.1

Kang, D., & Curchitser, E. N. (2015). Energetics of eddy-mean flow interactions in the gulf stream region. *Journal of Physical Oceanography*, *45*(4). https://doi.org/10.1175/JPO-D-14-0200.1

Keppler, L., & Landschützer, P. (2019). Regional Wind Variability Modulates the Southern Ocean Carbon Sink. *Scientific Reports*, *9*(1). https://doi.org/10.1038/s41598-019-43826-y

Martínez-Moreno, J., Hogg, A. M. C., Kiss, A. E., Constantinou, N. C., & Morrison, A. K. (2019). Kinetic Energy of Eddy-Like Features From Sea Surface Altimetry. *Journal of Advances in Modeling Earth Systems*. https://doi.org/10.1029/2019MS001769

Martínez-Moreno, J., Hogg, A. M., England, M. H., Constantinou, N. C., Kiss, A. E., & Morrison, A. K. (2021). Global changes in oceanic mesoscale currents over the satellite altimetry record. *Nature Climate Change*, *11*(5), 397–403. https://doi.org/10.1038/s41558-021-01006-9

Martínez-Moreno, J., Hogg, A. M. C., & England, M. H. (2022). Climatology, Seasonality, and Trends of Spatially Coherent Ocean Eddies. *Journal of Geophysical Research: Oceans*, *127*(7), e2021JC017453. https://doi.org/10.1029/2021JC017453

Mason, E., Pascual, A., & McWilliams, J. C. (2014). A new sea surface height-based code for oceanic mesoscale eddy tracking. *Journal of Atmospheric and Oceanic Technology*, *31*(5), 1181–1188. https://doi.org/10.1175/JTECH-D-14-00019.1

Menna, M., Cotroneo, Y., Falco, P., Zambianchi, E., Di Lemma, R., Poulain, P. -M., et al. (2020). Response of the Pacific Sector of the Southern Ocean to Wind Stress Variability From 1995 to 2017. *Journal of Geophysical Research: Oceans*, *125*(10), 1–18. https://doi.org/10.1029/2019JC015696

Meredith, M. P. (2016). Understanding the structure of changes in the Southern Ocean eddy field. *Geophysical Research Letters*, *43*(11), 5829–5832. https://doi.org/10.1002/2016GL069677

Meredith, M. P., & Hogg, A. M. (2006). Circumpolar response of Southern Ocean eddy activity to a change in the Southern Annular Mode. *Geophysical Research Letters*, *33*(16), L16608. https://doi.org/10.1029/2006GL026499

Morrison, A. K., Waugh, D. W., Hogg, A. M. C., Jones, D. C., & Abernathey, R. P. (2022). Ventilation of the Southern Ocean Pycnocline. *Annual Review of Marine Science*. https://doi.org/10.1146/annurev-marine-010419-011012

Orsi, A. H., Whitworth, T., & Nowlin, W. D. (1995). On the meridional extent and fronts of the Antarctic Circumpolar Current. *Deep-Sea Research Part I*. https://doi.org/10.1016/0967-0637(95)00021-W

Patara, L., Böning, C. W., & Biastoch, A. (2016). Variability and trends in Southern Ocean eddy activity in 1/12° ocean model simulations. *Geophysical Research Letters*, *43*(9). https://doi.org/10.1002/2016GL069026

Pedlosky, J. (1987). *Geophysical Fluid Dynamics*. *New York and Berlin, Springer-Verlag, 1982. 636 …*. New York, NY: Springer New York. https://doi.org/10.1007/978-1-4612-4650-3

Pegliasco, C., Chaigneau, A., & Morrow, R. (2015). Main eddy vertical structures observed in the four major Eastern Boundary Upwelling Systems. *Journal of Geophysical Research: Oceans*, *120*(9), 6008–6033. https://doi.org/10.1002/2015JC010950

Pegliasco, C., Delepoulle, A., Mason, E., Morrow, R., Faugère, Y., & Dibarboure, G. (2022). META3.1exp: a new global mesoscale eddy trajectory atlas derived from altimetry. *Earth System Science Data*, *14*(3). https://doi.org/10.5194/essd-14-1087-2022

Pujol, M. I., Faugère, Y., Taburet, G., Dupuy, S., Pelloquin, C., Ablain, M., & Picot, N. (2016). DUACS DT2014: The new multi-mission altimeter data set reprocessed over 20 years. *Ocean Science*, *12*(5). https://doi.org/10.5194/os-12-1067-2016

Rintoul, S. R. (2018). The global influence of localized dynamics in the Southern Ocean. *Nature*. https://doi.org/10.1038/s41586-018-0182-3

Samelson, R. M., Schlax, M. G., & Chelton, D. B. (2014). Randomness, symmetry, and scaling of mesoscale eddy life cycles. *Journal of Physical Oceanography*, *44*(3). https://doi.org/10.1175/JPO-D-13-0161.1

Scott, R. B., & Wang, F. (2005). Direct Evidence of an Oceanic Inverse Kinetic Energy Cascade from Satellite Altimetry. *Journal of Physical Oceanography*, *35*(9), 1650–1666. https://doi.org/10.1175/jpo2771.1

Screen, J. A., Gillet, N. P., Stevens, D. P., Marshall, G. J., & Roscoe, H. K. (2009). The role of eddies in the Southern Ocean temperature response to the southern annular mode. *Journal of Climate*, *22*(3). https://doi.org/10.1175/2008JCLI2416.1

Shi, J.-R., Talley, L. D., Xie, S.-P., Liu, W., & Gille, S. T. (2020). Effects of Buoyancy and Wind Forcing on Southern Ocean Climate Change. *Journal of Climate*, *33*(23), 10003–10020. https://doi.org/10.1175/JCLI-D-19-0877.1

Shi, J.-R., Talley, L. D., Xie, S.-P., Peng, Q., & Liu, W. (2021). Ocean warming and accelerating Southern Ocean zonal flow. *Nature Climate Change*, *11*(12), 1090–1097. https://doi.org/10.1038/s41558-021-01212-5

Straub, D. N. (1993). On the transport and angular momentum balance of channel models of the Antarctic Circumpolar Current. *Journal of Physical Oceanography*, *23*(4). https://doi.org/10.1175/1520-0485(1993)023<0776:OTTAAM>2.0.CO;2

Thompson, A. F., & Garabato, A. C. N. (2014). Equilibration of the Antarctic Circumpolar Current by standing meanders. *Journal of Physical Oceanography*, *44*(7). https://doi.org/10.1175/JPO-D-13-0163.1

Thompson, A. F., & Sallée, J. B. (2012). Jets and Topography: Jet Transitions and the Impact on Transport in the Antarctic Circumpolar Current. *Journal of Physical Oceanography*, *42*(6). https://doi.org/10.1175/JPO-D-11-0135.1

Tulloch, R., Marshall, J., Hill, C., & Smith, K. S. (2011). Scales, Growth Rates, and Spectral Fluxes of Baroclinic Instability in the Ocean. *Journal of Physical Oceanography*, *41*(6), 1057–1076. https://doi.org/10.1175/2011JPO4404.1

Venaille, A., Vallis, G. K., & Smith, K. S. (2011). Baroclinic turbulence in the ocean: Analysis with primitive equation and quasigeostrophic simulations. *Journal of Physical Oceanography*, *41*(9). https://doi.org/10.1175/JPO-D-10-05021.1

Viebahn, J., & Eden, C. (2010). Towards the impact of eddies on the response of the Southern Ocean to climate change. *Ocean Modelling*, *34*(3–4). https://doi.org/10.1016/j.ocemod.2010.05.005

Waugh, D. W., Primeau, F., DeVries, T., & Holzer, M. (2013). Recent changes in the ventilation of the southern oceans. *Science*. https://doi.org/10.1126/science.1225411

Youngs, M. K., Thompson, A. F., Lazar, A., & Richards, K. J. (2017). ACC meanders, energy transfer, and mixed barotropic-baroclinic instability. *Journal of Physical Oceanography*, *47*(6). https://doi.org/10.1175/JPO-D-16-0160.1

Zajaczkovski, U. (2017). *A study of the Southern Ocean: Mean state, eddy genesis & demise, and energy pathways*. University of California, San Diego.

Zhang, Y., Chambers, D., & Liang, X. (2021). Regional Trends in Southern Ocean Eddy Kinetic Energy. *Journal of Geophysical Research: Oceans*, *126*(6). https://doi.org/10.1029/2020JC016973